Hindawi
Journal of Nanomaterials
Volume 2022, Article ID 7964428, 15 pages
https://doi.org/10.1155/2022/7964428

Research Article

Evolution of Structural and Optical Properties of Cuprous Oxide Particles for Visible Light Absorption

A. R. Carrasco-Hernández,[1] **R. I. Ruvalcaba-Ontiveros**,[1] **E. Martínez-Guerra**,[2] **J. A. Duarte-Moller**,[3] **and H. E. Esparza-Ponce**[1]

[1]*Física de Materiales, Centro de Investigación en Materiales Avanzados S.C., Chihuahua, Chih. 31136, Mexico*
[2]*Unidad Monterrey, Centro de Investigación en Materiales Avanzados, S.C., Monterrey, N.L. 66600, Mexico*
[3]*División de Ciencias e Ingeniería, Universidad de Sonora, Unidad Regional Sur, Navojoa, Son. 85880, Mexico*

Correspondence should be addressed to H. E. Esparza-Ponce; hilda.esparza@cimav.edu.mx

Received 29 March 2022; Revised 6 July 2022; Accepted 25 July 2022; Published 1 September 2022

Academic Editor: Osman Ahmed Zelekew

Absorbent materials are being developed to replace semiconductor materials such as p-type silicon, GaAs, CdTe, and quaternary compounds such as CIGS (copper indium gallium selenide). Cu_2O is a potential candidate because it is non-toxic, inexpensive, an abundant compound in the Earth's crust, and has good optical properties, such as a high absorption coefficient. In this work, Cu_2O was obtained simply by reducing Benedict's solution with glucose in an alkaline medium (pH 10.2 ± 0.2) at 65°C. The samples were synthesized by varying glucose content from 1 g to 7 g. The results showed a phase proportion variation between 95.56% and 99.50% of the Cu_2O phase. It was found that the changes in crystallite size, microstrains, particle size, and morphology are due to reaction times, which were influenced by the use of different glucose amounts. The use of a higher glucose amount in the synthesis favors a faster reaction, forming smaller crystallites with more microstrains. Lower glucose amount leads to a slower reaction giving the crystallites more time to grow, which relaxes the microstrains. When increasing glucose content, the obtained morphologies changed from cubes, irregular cubes, prismatic spheres, cauliflower-like, to spherical shapes. The XPS spectra confirmed only the presence of chemical species such as Cu(I) and Cu(II), and chemical defects, such as oxygen vacancies (*Vo*), were detected in the samples. All samples presented a broad absorption range from 200 nm to 570 nm indistinctly of the morphology. The band gap showed an insignificant change from 2.04 eV to 2.09 eV when glucose was increased from 1 g to 7 g. The *in-situ* phase transformation study was analyzed from 25°C to 700°C. The results indicated a phase transition from Cu_2O to Cu and CuO when the temperature was above 280°C.

1. Introduction

The increasing energy demand and environmental problems, such as contamination from the combustion of fossil fuels, [1] have brought the need to use alternative energy sources for energy production [2, 3]. Cu_2O is a promising candidate for photovoltaic applications as a possible solution to the global energy crisis [1, 4], providing alternative, safe, and sustainable energy sources [3]. Examples of this are the conversion of solar energy into electrical energy [5–7] and the generation of hydrogen from the photoelectrochemical conversion of the sun [3, 8].

In recent years, the research has been focused on the search for emerging cheap materials that are abundant in the Earth's crust, non-toxic, and have structural, optical, and electrical properties that make them adequate as light-absorbing materials [9]. Cu_2O is a p-type semiconductor due to the negatively charged Cu vacancies [10]. It has a direct band gap between 1.9 and 2.2 eV [11, 12] and a significant absorption coefficient from violet to green in the range of the solar spectrum ($\alpha = 4 \times 10^3$ cm^{-1} at 600 nm) [13, 14].

Cuprous oxide is used in electrodes for lithium-ion batteries, photochemical cells, hydrogen production, sensors, photocatalysts, supercapacitors, magnetic storage, and water

splitting [15–21], as well as a bactericide, colorant, and additive for corrosion-proof coatings [22–24]. Various methods have been developed to obtain Cu_2O, such as the water bath method, the SILAR (Successive Ionic Layer Absorption and Reaction) method, the polyol method, chemical reduction, and sol-gel [4, 10, 17, 25–32]; however, some of these methods require special equipment [17, 27, 28], catalysts, organic additives, or expensive surfactants [25, 31, 32].

Among the available methods, the reduction of copper salts with some reducing agents has been identified as a simple process with a quick reaction rate [4, 16, 28]. The use of glucose as a reducing agent has the advantage of being environmentally friendly, resulting in green chemical synthesis. Besides, glucose is cheap and highly selective in producing Cu_2O [24, 33], and its use is suitable for the development of Cu_2O particles with different morphologies like spheres, cubes, beveled cubes, octahedrons, flower shapes, nanowires, nanorods, hierarchical structures, cages, and hollow structures [17, 25, 34, 35] by changing the temperature, pH, reagents, solvents, reaction times, and surfactants control [36–43].

Over the years, several works have reported the formation of Cu_2O using glucose as a reducing agent. In 2009, for example, Cao and colleagues investigated the effect of the synthesis temperature on the morphological evolution of Cu_2O particles. Their study focused on synthesis temperatures from 95°C to 180°C using an autoclave system and reaction times from 6 to 36 hours. They found qualitatively that at synthesis temperatures above 180°C, they obtained a mixture of Cu_2O and metallic copper [44]. On the other hand, Cao et al. [44] reported the formation of different morphologies of Cu_2O by varying the glucose concentration at a synthesis temperature of 50°C. They observed qualitatively the appearance of CuO peaks in their diffraction patterns when the glucose concentration is deficient, suggesting that the reduction of Cu^{+2} ions into Cu^{+1} ions is not complete under low glucose conditions [45].

In this work, Cu_2O was obtained by reducing Benedict's solution with glucose in an alkaline medium (pH ~ 10.2 ± 0.2) without any surfactants, additives, or templates. Our work avoids using sulfur-containing reagents or any special equipment; instead, we developed a rapid and simple synthesis at a low temperature of 65°C. The present study mainly focuses on the effects of the glucose content and the temperature on structural and optical properties. A detailed quantitative analysis was carried out using the Rietveld refinement and the Williamson-Hall (W-H) approach to quantify the composition of the samples and to obtain structural information such as the variation of lattice parameters, crystallite size, unit cell volume, and microstrains. The results showed a mixture of phases in the composition of the samples. In addition, when the glucose content increased, the crystallite size decreased, and the microstrains increased. Various morphologies were obtained when the amount of reducing agent was changed. However, all morphologies showed an absorption broad almost constant in the range of 200 nm to 570 nm. The *in-situ* X-ray diffraction showed that Cu_2O transforms to Cu at temperatures above 300°C and CuO at temperatures above 320°C. These properties make Cu_2O a candidate for solar cell applications as a light absorber material.

2. Experimental Details

2.1. Materials. The reagents used for Cu_2O synthesis were cupric nitrate hemipentahydrate, $Cu(NO_3)_2{\cdot}2.5H_2O$ (98.9% purity, Fisher Chemical), sodium carbonate anhydrous, Na_2CO_3 (99.5% purity, J. T. Baker), sodium citrate dihydrate, $C_6H_5Na_3O_7{\cdot}2H_2O$ (99% purity, J. T. Baker), and D-(+)-glucose anhydrous, $C_3H_{12}O_6$ (99% purity, Alfa Aesar). All reagents were of analytical grade and not further purified.

2.2. Synthesis of Cu_2O Particles. Benedict's solution was prepared by dissolving 0.80 g of $Cu(NO_3)_2{\cdot}2.5H_2O$, 5.0 g of Na_2CO_3, and 10.0 g of $C_6H_5Na_3O_7{\cdot}2H_2O$ in 50 mL of deionized water, yielding a dark blue solution with pH about 10.2 ± 0.2. Then, the solution was heated to 65°C with constant stirring, and 1-7 g (0.11 M to 0.77 M) of anhydrous D-(+)-glucose was added. The stirring and the temperature were maintained for 10 min, and then, the solution was cooled naturally to room temperature. The orange precipitates were collected by centrifugation at 6000 rpm for 5 min. They were washed three times with deionized water to remove any residue produced in the reaction. The centrifuged powders were dried at room temperature for 24 h.

2.3. Characterization. X-ray diffraction was performed using a PANalytical X'pertPRO diffractometer with Cu Kα1 radiation (λ_{Cu} = 1.541874 Å). The scan range was from 20° to 80°, and the step size was 0.017°. The XRD patterns were refined on the Fullprof software [46] using the Rietveld method. The crystallite size and microstrains were calculated by Rietveld refinement and the W-H approach. The morphologies and chemical compositions were determined by scanning electron microscopy (SEM) and energy dispersive spectroscopy (EDS), respectively, on a JSM-7401F JEOL microscope. XPS measurements were performed in the ESCALAB 250Xi photoelectron spectrometer ultrahigh vacuum chamber with a monochromatic Al kα source (1486.7 eV). Peaks were deconvoluted using CasaXPS software [47]. The absorbance was measured in the UV-visible region using diffuse reflectance spectroscopy (DRS) on an Evolution 220 Thermo Scientific spectrometer with a 1 nm spectral bandwidth in the wavelength range of 200 nm to 800 nm. The band gap was estimated from Tauc's graphs according to the Kubelka-Munk theory by extrapolation of the straight line. Finally, the *in-situ* phase transformation was studied under the above experimental conditions in a temperature range from 25°C to 700°C.

3. Results and Discussion

The XRD patterns in Figure 1(a) reveal a cubic crystal structure with a $Pn\bar{3}m$ space group. The cubic structure of Cu_2O was indexed by PDF card No. 77-0199. All samples have seven characteristic reflections corresponding to the crystallographic planes (110), (111), (200), (211), (220), (311), and

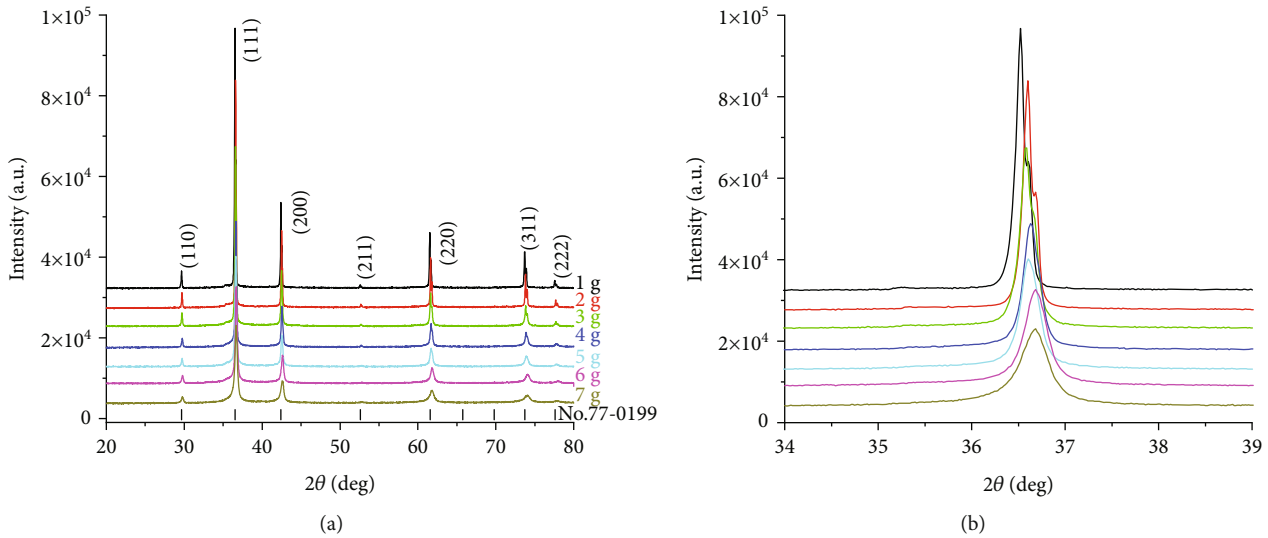

FIGURE 1: (a) XRD patterns of Cu_2O particles synthesized with different amounts of glucose and (b) enlarged pattern of the reflection peak (111) of Cu_2O.

(222) of Cu_2O. The peaks of the samples with the lowest glucose content are high and narrow, indicating high crystallinity. On the other hand, it can be observed in the inset in Figure 1(b) that the reflection belonging to the plane (111) shows a significant broadening (full width at half maximum, or FWHM) and a slight shift to the right as the glucose content increases. The broadening indicates a decrease in crystallite size, and the shift to the right can be caused by microstrains in the lattice.

The fitting of the experimental XRD data to quantify the phases, lattice parameters, and unit cell volume was performed using the pseudo-Voigt function of the peak profile and the least-squares convergence criterion. The pseudo-Voigt function is determined by:

$$f_{pV} = \eta G + (1 - \eta) \bullet L, \tag{1}$$

where f_{pV} is the pseudo-Voigt function, η describes how Gaussian or Lorentzian the peak shape is, G is the Gaussian contribution, and L is the Lorentzian contribution to the peak shape [46].

The samples synthesized with the lowest glucose content showed a small peak belonging to the monoclinic tenorite phase (CuO). Therefore, two phases were proposed in the composition of the samples (Cu_2O and CuO). The quantification of the phases, chi-square (goodness of fit), R factors such as R_{pw} (weighted profile factor) and R_{exp} (expected factor), lattice parameters, and unit cell volume are summarized in Table 1. According to the values of X^2, the refinements show good agreement with the experimental data ($1.05 \leq X^2 \leq 1.70$). All samples present a monoclinic CuO phase ranging from 0.50% to 5.44%, which increases with the decrease of glucose content. The fit between the experimental data and the data calculated by Rietveld refinement is shown in Figure 2. For clarity, only the samples synthesized with 1 g and 7 g of glucose were shown. The sample synthesized with 7 g glucose has a composition of 99.50% Cu_2O and 0.50% CuO with a standard deviation of 0.34% and 0.01%, respectively, which means that the largest proportion of the sample corresponds to the Cu_2O phase. Lattice parameters and unit cell volume of all samples are also shown in Table 1. It can be seen that there is a clear tendency in both parameters to decrease when the glucose content increases, which verifies the shift to the right of the reflection peak (111) observed in Figure 1(b). The lattice parameters are 4.2602 Å to 4.2459 Å for the samples synthesized with 1 g and 7 g of glucose and are similar to those reported in the literature [9, 25, 48].

Crystallite size and microstrains were also determined using Rietveld refinements. In contrast to the refinements shown above, the procedure to determine the crystallite size and microstrains changes. In this case, the Thompson-Cox-Hastings (TCH) pseudo-Voigt model was used, which accounts for the contributions of crystallite size and microstrains to the peak broadening. In contrast, the Scherrer equation only considers the effect of crystallite size on the total broadening of the diffraction peak but says nothing about the microstructures of the lattice, i.e., the intrinsic microstrains [49, 50]. The crystallite size and the microstrains are calculated with the following formulas:

$$\text{Crystallite size} = \frac{1}{\beta_{\text{size}}} \left[\text{Å}\right], \tag{2}$$

$$\text{Max}_{\text{strain}} = \frac{1}{2} \beta_{\text{strain}} d_{\text{hkl}} \left[10^{-4}\right], \tag{3}$$

Table 1: Rietveld refinement data of Cu_2O samples synthesized with various amounts of glucose.

Glucose [g]	Quantification of phase [%] Cu_2O	CuO	X^2	R_{pw}	R_{exp}	Lattice parameter [Å]	Unit cell volume [Å]
1	94.56 ± 0.23	5.44 ± 0.01	1.48	7.30	6.00	4.26020 ± 0.00013	77.320 ± 0.004
2	98.07 ± 0.48	1.93 ± 0.05	1.70	7.35	5.64	4.25734 ± 0.00014	77.164 ± 0.004
3	98.48 ± 0.25	1.52 ± 0.03	1.40	8.00	6.76	4.25505 ± 0.00017	77.040 ± 0.005
4	98.61 ± 0.28	1.39 ± 0.03	1.45	9.22	7.65	4.25463 ± 0.00034	77.017 ± 0.011
5	98.73 ± 0.73	1.27 ± 0.03	1.27	8.72	7.73	4.25290 ± 0.00047	76.923 ± 0.015
6	99.17 ± 0.33	0.83 ± 0.01	1.05	8.04	7.84	4.24611 ± 0.00058	76.555 ± 0.018
7	99.50 ± 0.34	0.50 ± 0.01	1.07	8.02	7.77	4.24597 ± 0.00104	76.547 ± 0.033

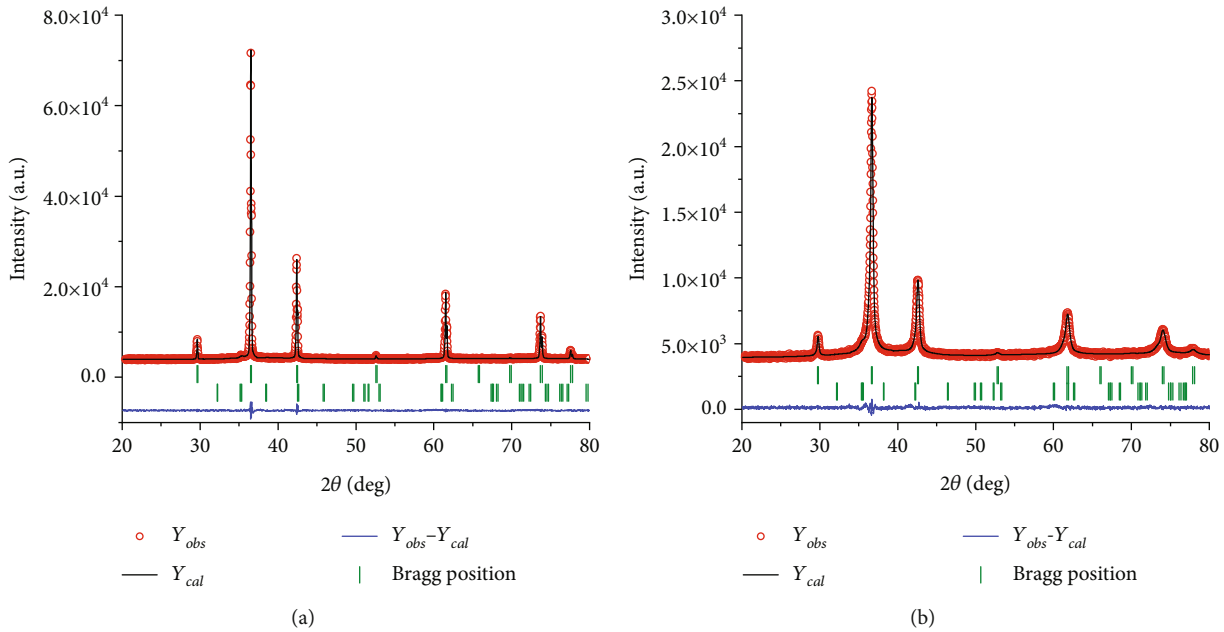

Figure 2: Rietveld refinement of the samples synthesized with (a) 1 g and (b) 7 g glucose.

where β_{size} is the peak broadening due to crystallite size. β_{size} is obtained as follows:

$$\mathrm{FWHM}^2(G_{\mathrm{size}}) = H_G^2 = \frac{I_G}{\cos^2\theta},$$
$$\mathrm{FWHM}(L_{\mathrm{size}}) = H_L = \frac{[Y + F(S_z)]}{\cos\theta}, \quad (4)$$

where H_G and H_L are the $FWHM$ of the Gaussian and Lorentzian components, respectively, and θ is the diffraction angle. For the calculation of the anisotropic model, I_G is the Gaussian mixing parameter, Y is set to zero, and $F(S_Z)$ is the function of the anisotropic broadening contribution by crystallite size.

From Equation (3), d_{hkl} is the interplanar distance, and β_{strain} is the peak broadening due to microstrains calculated by:

$$\mathrm{FWHM}^2(G_{\mathrm{strain}}) = H_G^2 = \left[U + (1-\xi)^2\mathrm{DST}^2\right]\tan^2\theta,$$
$$\mathrm{FWHM}(L_{\mathrm{strain}}) = H_L = [X + \xi\mathrm{DST}]\tan\theta, \quad (5)$$

where for the calculation of the anisotropic model, U and X are set to zero, ξ is a mixing coefficient to Lorentzian contribution, and DST is the function of the anisotropic broadening contribution by microstrains. Both crystallite size and microstrains take into account the spherical harmonics [46].

Crystallite size and microstrains were also calculated using W-H analysis. The simple W-H approach has some variants, such as the uniform deformation model (UDM), the uniform stress deformation model (USDM), and the

uniform deformation energy density model (UDM) [49]. In the present work, the UDM approach was used. Like Rietveld, Williamson and Hall attribute the broadening of the peak shape to crystallite size and microstrains. Therefore, it is stated that:

$$\beta = \beta_{\text{size}} + \beta_{\text{strain}}, \tag{6}$$

where β is de FWHM, β_{size} is the broadening by crystallite size, and β_{strain} is the broadening attributed to microstrains. Through the W-H method, it is possible to separate these effects as follows:

$$\beta \cos\theta = \frac{k\lambda}{L} + 4\varepsilon \sin\theta, \tag{7}$$

where L is the crystallite size, ε is the value of microstrains, k is a constant [0.9], and λ is the wavelength of the incident ray [$\lambda_{Cu} = 1.541874$ Å]. As seen in Equation (7), the result is the straight line equation. The first term corresponds to the crystallite size broadening, and the second term corresponds to the microstrains broadening. This method consists of plotting $\beta \cos\theta$ vs. 4 $\sin\theta$, where the slope provides information on the microstrains, while the intercept explains the crystallite size [49, 50].

Figure 3 shows the crystallite size and microstrains calculated by (a) Rietveld refinement and (b) the W-H approach. The average crystallite size for the Rietveld refinement is 2045 Å for the sample synthesized with 1 g of glucose, while the average crystallite size for the sample synthesized with 7 g of glucose is 137 Å. In the W-H case, the crystallite size is about 964 Å and 341 Å for the sample synthesized with 1 g and 7 g of glucose, respectively. A clear trend of decreasing crystallite size with increasing glucose is observed in both calculations, confirming the peak broadening (FWHM) in the XRD data.

Microstrain values (red line with squares) are found to increase with the increase in glucose content. A value of 4.89×10^{-4} was obtained by Rietveld refinement for the sample synthesized with 1 g of glucose and 65.3×10^{-4} for 7 g of glucose. The W-H approach shows a value of 1.05×10^{-4} for the sample containing 1 g of glucose and 25.9×10^{-4} for the sample containing 7 g of glucose.

From Figure 3, the W-H analysis's crystallite size and microstrains are smaller than the crystallite size and microstrains calculated by the Rietveld refinement. The UDM method used in the present work assumes that the microstrains are uniform in all crystallographic directions. UDM considers the isotropic nature of the crystal, where the material properties are independent along any direction in which they were measured [49, 51]. In contrast, UDSM and UDEDM assume that the crystals are anisotropic [52]. Therefore, the discrepancy between the two methods can be attributed to the fact that W-H (UDM used in this work) assumes an isotropic nature of the sample, and Rietveld considers anisotropy.

To determine the Cu_2O formation and to confirm the composition of the samples, the formation mechanism was established as follows:

$$Cu^{+2} + (C_6H_5O_7)^{-3} \longrightarrow \text{Cu•citrate(complex)}, \tag{8}$$

$$\text{Cu•citrate (complex)} + (CO_3)^{-2} \longrightarrow 2Cu(OH)_2, \tag{9}$$

$$2Cu(OH)_2 + C_6H_{12}O_6 \longrightarrow Cu_2O{\downarrow} + C_6H_{12}O_7 + 2H_2. \tag{10}$$

In this redox reaction, cupric nitrate acts as an oxidizing agent; sodium citrate stabilizes the Cu^{+2} ions from cupric nitrate; sodium carbonate alkalizes the medium; and glucose acts as a reducing agent. First, in Benedict's solution, the cupric nitrate is dissolved in water forming a uniform ionic solution. Then, the citrate ions coordinate with Cu^{+2} ions to form the water-soluble Cu-citrate complex [45] (Equation (8)). When carbonate is added to the solution, the Cu^{+2} ions react with the OH^- ions to form blue water-insoluble $Cu(OH)_2$ (Equation (9)).

Finally, when the reacting agent (glucose), which contains aldehyde groups (R-CH=O), is introduced into the solution, the aldehyde groups of the glucose molecules cause the reduction of Cu^{+2} into Cu^{+1} ions. This results in the formation of Cu_2O as an orange precipitate and the oxidation of the aldehyde to a carboxylic acid [53, 54] (Equation (10)). The higher the glucose content in the solution, the more aldehyde groups will be present in the reaction. This means that a larger amount of Cu^{+2} ions will be reduced to Cu^{+1} by glucose aldehydes. Therefore, the Cu^{+2} ions of $Cu(OH)_2$ are completely consumed and reduced to Cu^{+1} ions forming Cu_2O.

Nevertheless, when a small amount of glucose is added, the Cu^{+2} ions from $Cu(OH)_2$ are not completely reduced, and they remain as Cu^{+2} ions [32], forming CuO. These findings agree with those of Cao [45], who in 2010 discovered a low percentage of the CuO phase when they had an atmosphere lacking in glucose. Rietveld refinement confirms that the sample with the higher glucose content has the highest amount of the Cu_2O phase.

The evolution of all samples' morphology and chemical composition is shown in Figure 4. The morphology takes different shapes with changes in the glucose content. Figures 4(a) and 4(b) show cubes and irregular shapes clustered from smaller cubes with well-defined edges and corners. The average length of the edge of the cubes is about 876 nm and 903 nm for the samples synthesized with 1 g and 2 g of glucose, respectively. When the glucose increases to 3 g, a mixture of cubes and prismatic structures in a ratio of about 1 : 1 can be seen (Figure 4(c)), which is similar to the results of Liang et al. in 2015 [25]. The average length of the edge of the cubes is about 686 nm, while the average diameter of the prismatic structures is 892 nm. When the glucose increases to 4 g (Figure 4(d)), bulging cubes with an average particle size of 864 nm can be seen. In Figure 4(e), the morphology of the sample synthesized with 5 g of glucose resembles a cauliflower with an average diameter of 899 nm. Finally, at 6 g and 7 g of glucose, a

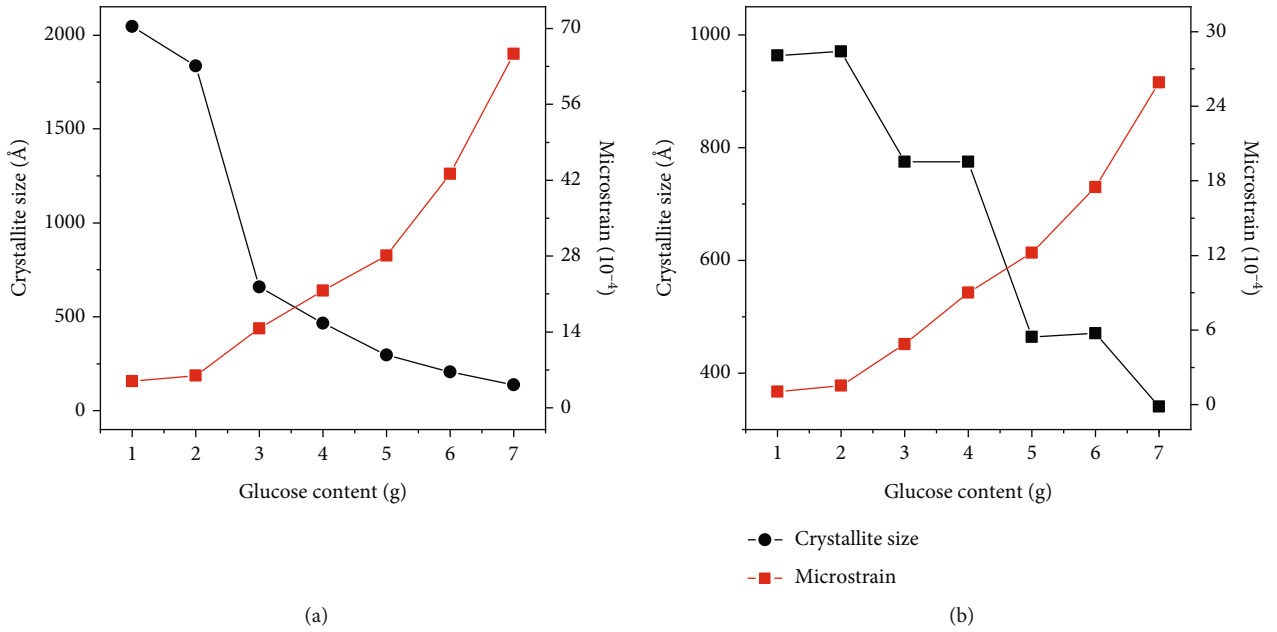

Figure 3: Crystallite size and microstrains of Cu_2O samples synthesized with different amounts of glucose by (a) Rietveld refinement and (b) W-H approach.

semispherical morphology with slight surface roughness is observed (Figures 4(f) and 4(g)) with average diameters of 635 nm and 687 nm, respectively. The histograms of particle size distribution are shown to the right of each SEM image. Each histogram indicates the samples' average particle size and standard deviation. It was found that particle size decreases with the increase in glucose content.

EDS analysis shows Cu and O as the only elements present in the samples, confirming the absence of impurities. The atomic percentages of both elements are shown in Table 2. It is noticeable that the samples synthesized with 5 g, 6 g, and 7 g of glucose show approximately the theoretical ratio of 2 : 1. The increase in Cu signal in samples synthesized with 1 g to 4 g of glucose could be related to a higher proportion of CuO secondary phase.

It was found that the increase in the glucose amount in the synthesis affected the reaction rate. The higher amount of glucose, the more aldehyde groups (R-CH=O) are present in the solution. Namely, the aldehydes from glucose react faster with Cu^{+2} ions and reduce them to Cu^{+1} ions. Consequently, the solution with less glucose has a slower reaction rate, similar to the observations presented by Amudhavalli et al. in 2018 [10]. In this work, the reaction times were~240 s (1 g), ~210 s (2 g and 3 g), ~180 s (4 g and 5 g), ~140 s (6 g), and~120 s (7 g). By those times, the solutions turned orange, indicating the formation of Cu_2O. When there is a low amount of glucose in the solution, the reduction rate of Cu^{+2} to Cu^{+1} is relatively low. It is situated in dislocation growth leading to the formation of cubic particles [45]. A slower reaction gives the crystallites enough time to grow [34], which leads to the formation of larger crystallites with smaller microstrain values confirming the Rietveld refinement and W-H approach. According to the literature, a slow reaction rate favors the growth along the <100> direction when compared to the <111> direction, leading to the formation of cubic particles [34]. This can be observed in the samples synthesized with 1 g and 2 g of glucose, which have a cubic morphology with an average particle size of 876 nm and 903 nm, respectively. When there is an excess of glucose in the solution, the reduction rate of Cu^{+2} to Cu^{+1} accelerates. In this case, the aggregation growth mode becomes dominant, and spherical particles are obtained [45]. A faster reaction induces a smaller crystallite size due to the rapid termination of crystallite formation [34]. This leads to the formation of microstrains with a higher value, which agrees with Rietveld's refinement and W-H analysis. At the fastest reaction time of 120 s, there is not enough time for the particles to grow in any specific direction. Therefore, spherical particles with smaller sizes of 635 nm and 687 nm are formed, as seen in Figures 4(f) and 4(g). The results of Cao et al. [44] and Cao et al. [45] are similar to those reported in the present work. However, unlike these two studies, our work does not use sulfur-containing reagents. The synthesis in our work is simple and needs only one hot plate. It is also fast, with short synthesis times at a low temperature of 65°C, and it contains a detailed study of structural properties by Rietveld refinement and the W-H approach.

XPS study was performed to observe the chemical species present in the samples. The spectra were analyzed using CASAXPS software. The Shirley-type background, mainly used for metal analysis, was also determined [47] with the line shape LF (Lorenztian-Gaussian). Finally, the spectra fitting was performed using the Marquardt least-squares method [55], and the peak positions were calibrated using the C 1 s peak, which standard binding energy is about 284.5 eV [56].

The XPS spectra of the samples synthesized with different amounts of glucose are shown in Figure 5. It can be seen from Figure 5(a) that all the spectra consist of two main

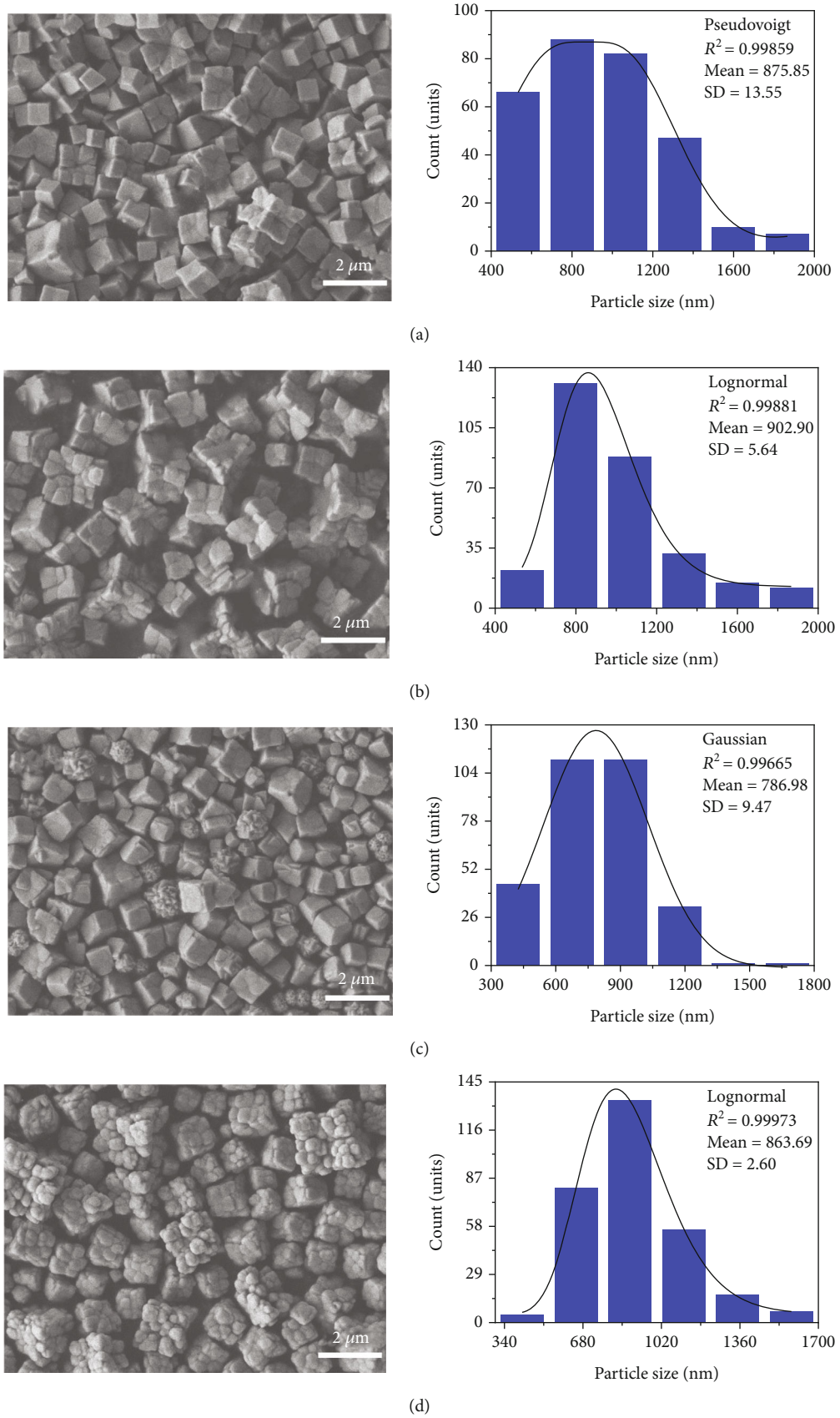

Figure 4: Continued.

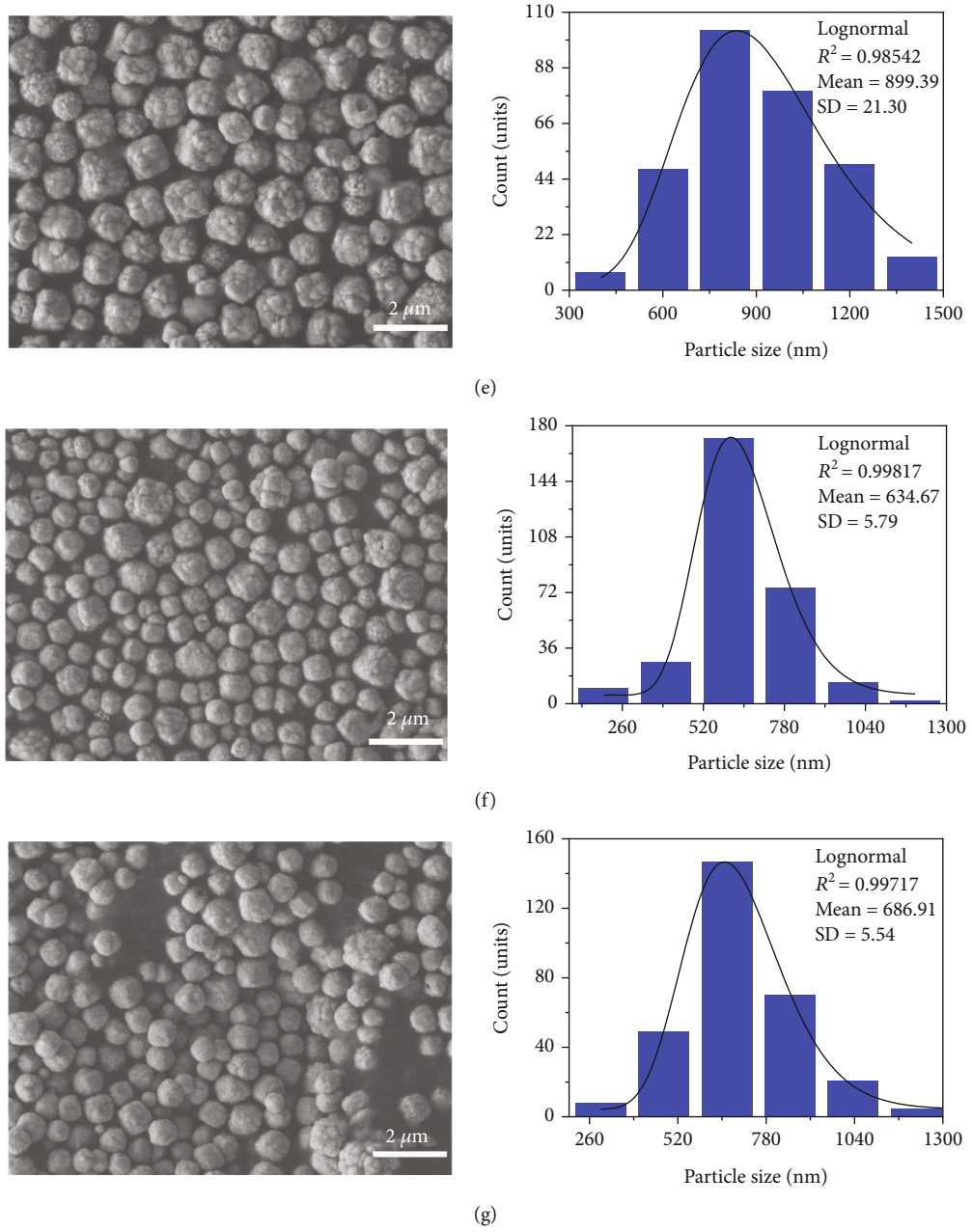

Figure 4: SEM images of Cu_2O samples synthesized with (a) 1 g, (b) 2 g, (c) 3 g, (d) 4 g, (e) 5 g, (f) 6 g, and (g) 7 g of glucose with their respective particle size distribution. An average of 300 particles was measured for the particle size distribution.

Table 2: EDS analysis of Cu_2O samples synthesized with different amounts of glucose.

Glucose [g]	Atomic percentage (%)		Ratio
	Cu	O	
1	73.24	26.76	2.7 : 1
2	71.13	27.87	2.6 : 1
3	70.05	29.95	2.3 : 1
4	72.00	28.00	2.6 : 1
5	67.01	32.97	2.0 : 1
6	65.50	34.45	1.9 : 1
7	66.56	33.44	2.0 : 1

peaks due to the spin-orbit splitting of Cu 2p (Cu $2p_{1/2}$ and Cu $2p_{3/2}$). The first peak is attributed to Cu $2p_{1/2}$ centered at 952.30 eV, and the second peak is attributed to Cu $2p_{3/2}$ centered at ~932.40 eV. These values are similar to those reported in the literature [33, 57]. However, the samples show satellite peaks around 940-945 eV and 960-966 eV [17, 56], which are from CuO signals [56]. Thus, the spectra indicate that the samples are dominated by Cu^{+1} (Cu(I) species) with the presence of Cu(II) species since the shoulders at 932 eV and 955 eV assigned to Cu^{+2} are not observed. However, the presence of the CuO phase (Cu(II) species) is confirmed by the detection of the satellites [17]. In Figure 5(a), it is observed that the intensity of the satellite

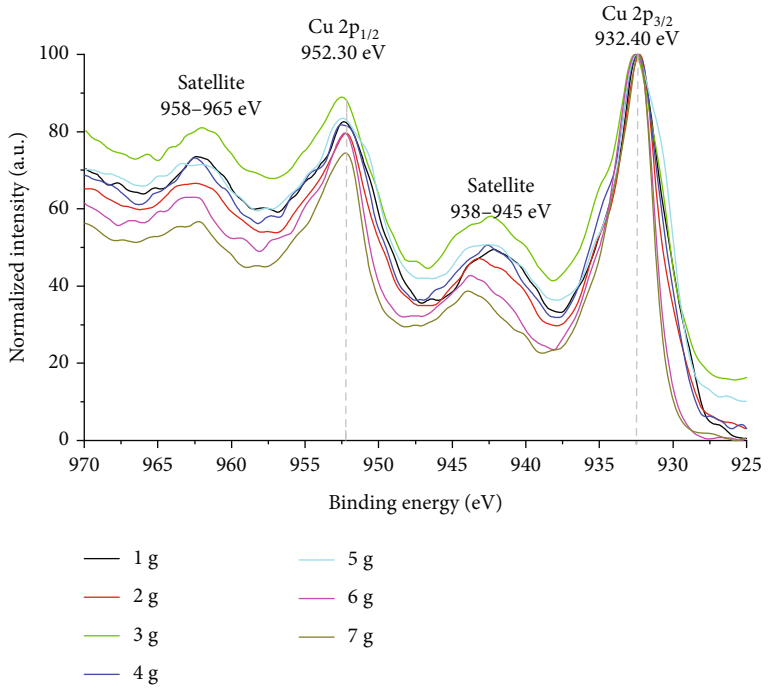

(a)

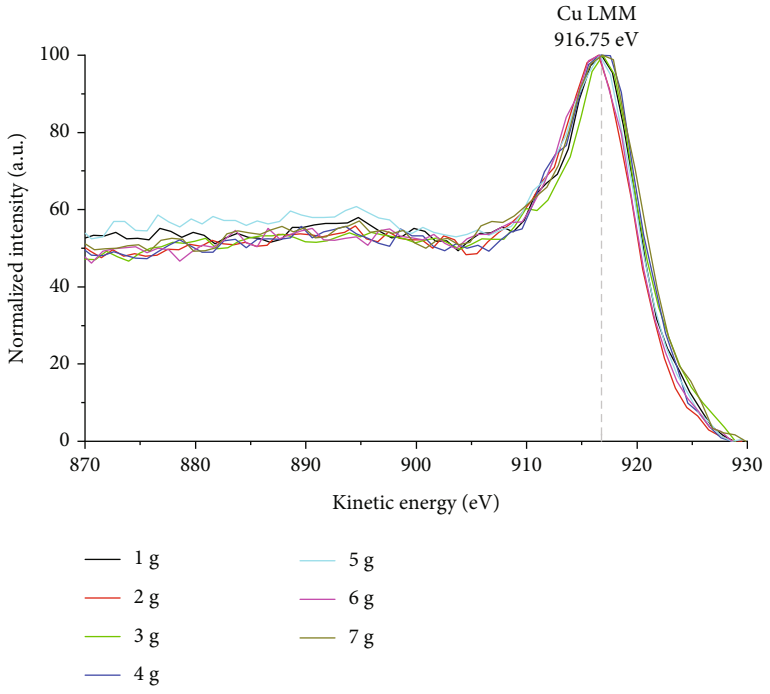

(b)

Figure 5: Continued.

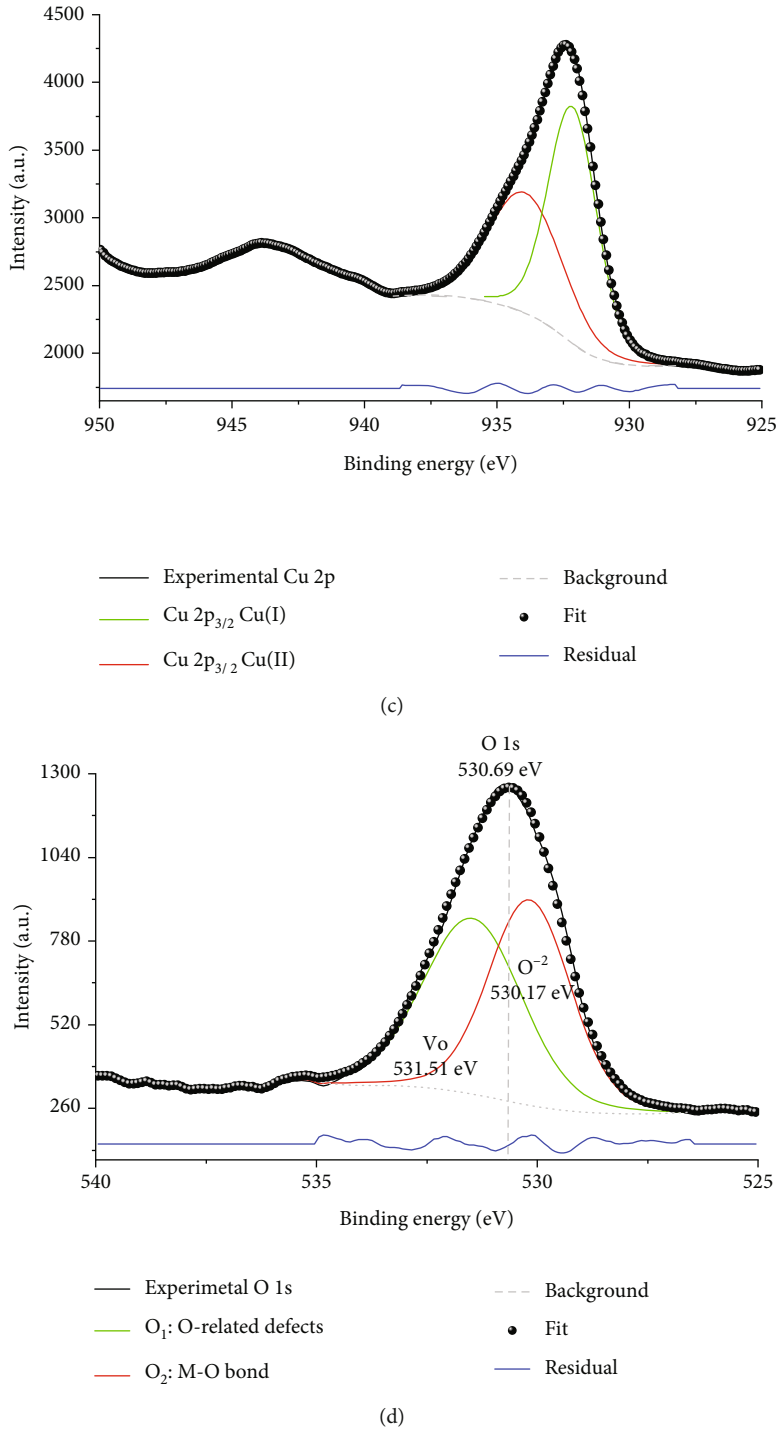

FIGURE 5: (a) XPS Cu 2p, (b) Cu LMM spectra of Cu_2O particles synthesized with different amounts of glucose, (c) XPS Cu $2p_{3/2,}$ and (d) O 1s spectrum of the sample synthesized with 7 g glucose.

decreases with the increase of the glucose content, suggesting a decrease in CuO content [56].

In general, the determination of chemical species such as Cu(0) and Cu(I) from Cu 2p spectra is not possible because the binding energy values are very close [58, 59]. However, it can be determined using the position and shape of the Cu LMM Auger peak, similar to those reported in 2016 by Devaraj et al. [58] and Biesinger et al. in 2017 [59].

The Auger peak position of Cu(0) should occur at 918.7 eV with shoulders on both sides [59]. Therefore, a visual examination of the overall peak shape of Cu LMM is shown in Figure 5(b). The Auger peak is observed at

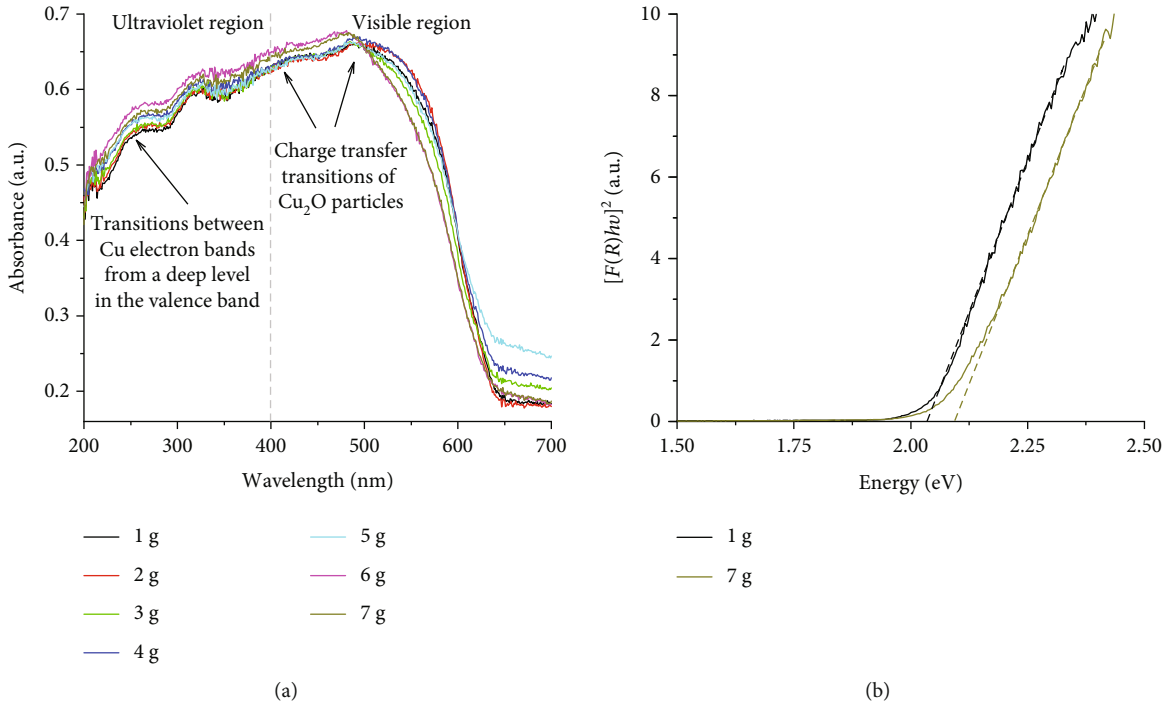

FIGURE 6: (a) Absorbance spectra of Cu_2O samples synthesized with different amounts of glucose and (b) estimation of the band gap by the Tauc plot for the samples synthesized with 1 g and 7 g glucose.

916.5 eV without shoulders on either side, indicating that no Cu(0) is present in the samples.

Figures 5(c) and 5(d) show the XPS spectra of the Cu $2p_{3/2}$ and O 1s peaks of the sample synthesized with 7 g glucose. Figure 5(c) shows that two components were fitted to the Cu $2p_{3/2}$ peak. The first component centered at 932.25 eV is attributed to Cu(I) species, and the second component centered at 934.05 eV belongs to Cu(II) species which is similar to what Meda et al. reported [60]. The XPS spectrum of O 1 s is shown in Figure 5(d). Fitting was performed with two components for this peak. The first peak is due to metal-oxygen bonds (Cu-O) centered at 530.15 eV, and the second is due to oxygen-related defects, such as oxygen vacancies (*Vo*), centered at 531.55 eV. In general, the metal-oxygen peaks and the oxygen-related defect peaks in metal oxides are near 530.6 eV and 531.9 eV, respectively [56], similar to those found in this work.

Figure 6(a) displays the absorption spectra of the Cu_2O samples. A broad absorption range from 200 nm to 570 nm can be seen. Usually, the broadening of the absorption peak is attributed to enhance light scattering caused by a decrease in the crystallite size and inhomogeneous particle size [25, 37, 61]. The results presented in this work show no significant effect in the absorption range when changing the glucose content or particle morphology. The characteristic transitions of Cu_2O in the absorption peaks were observed. The absorption at ~270 nm in the ultraviolet region is attributed to transitions between Cu electron bands from a deep level in the valence band [37]. The absorption bands between 340 nm and 440 nm in the visible region and at ~485 nm are attributed to charge transfer transitions of Cu_2O particles [61]. No absorption bands of Cu or CuO are observed. The surface plasmon band of metallic copper is generally in the range of 570 nm to 600 nm. At the same time, the charge transfer transitions of CuO are observed at wavelengths longer than 650 nm [62]. Therefore, a small percentage of CuO in the samples does not affect the absorption spectra significantly.

The band gap diagrams for the samples synthesized with 1 g and 7 g of glucose can be found in Figure 6(b). The band gap energy (Eg) was determined by applying the Kubelka-Munk function:

$$\frac{K}{S} = \frac{(1-R)^2}{2R} = F(R), \tag{11}$$

where K is the absorption coefficient, S is the scattering coefficient, R is the value of reflectance, and $F(R)$ is the Kubelka-Munk function. The band gap energy and the absorption coefficient are related through the Tauc relation described by the expression:

$$[F(R)\mathrm{h}\nu]^2 = A(\mathrm{h}\nu - \mathrm{Eg})^2, \tag{12}$$

where $h\nu$ is the photon energy, A is a proportionality constant, Eg is the band gap, and γ is 1/2 for direct band gap materials. The graph of $[F(R)]^2$ versus $h\nu$ was obtained by extrapolating the straight line to the zero intercept [63]. The band gap is in the range of $2.04 \leq \mathrm{Eg} \leq 2.09$ eV and increases slightly with the rise of glucose content. This difference is explained by the effect of the particle size due to quantum confinement, i.e., the generation of discrete energy levels in the valence and the conduction bands [21, 40, 64].

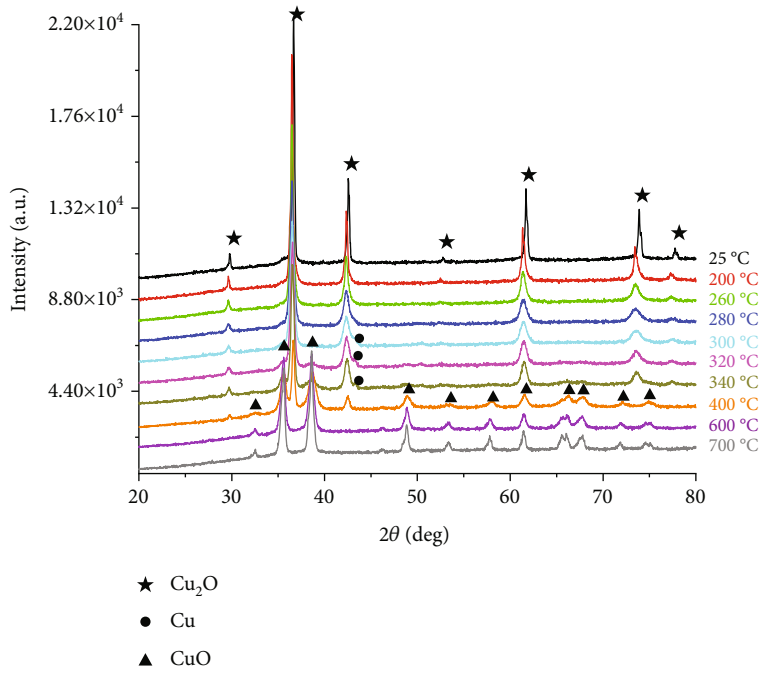

Figure 7: XRD patterns *in-situ* as a function of temperature.

Table 3: Rietveld refinement data of phase transformation study in function of the temperature.

Temperature [°C]	Quantification of phase [%]			X^2	R_{pw}	R_{exp}
	Cu_2O	CuO	Cu			
25	98.48 ± 0.25	1.52 ± 0.03	0.00	1.40	8.00	6.76
200	98.48 ± 0.48	1.52 ± 0.10	0.00	1.78	14.90	11.16
260	98.04 ± 1.09	1.96 ± 0.64	0.00	1.01	10.90	10.92
280	92.62 ± 1.39	0.67 ± 0.07	6.70 ± 0.24	1.14	12.68	11.87
300	89.08 ± 2.08	4.89 ± 0.29	6.02 ± 0.37	1.29	14.44	12.69
320	84.16 ± 1.83	13.28 ± 0.42	2.56 ± 0.07	1.17	14.60	13.47
340	69.44 ± 1.70	29.19 ± 0.54	1.37 ± 0.20	1.20	14.70	13.40
400	45.49 ± 3.35	54.51 ± 2.06	0.00	2.13	18.75	12.82
600	0.00	100.00	0.00	1.80	15.81	11.76
700	0.00	100.00	0.00	1.81	14.81	11.00

The reduction in particle size leads to an increase in the band gap of the material, which shows a blue shift similar to what is reported in the literature [12, 21]. However, for the band gap values in this work, the increase is only 0.05 eV, which could be negligible due to experimental error. The band gap values are similar to those published in the literature [11], thus confirming the Cu_2O phase. It was found that the evolution of the morphology, crystallite size, and particle size has no significant effect on spectral absorption or band gap estimation.

A phase transformation study from Cu_2O powders as a function of temperature was carried out to observe the stability of Cu_2O. The phase transformation analysis is shown in Figure 7 for the sample synthesized with 3 g of glucose. Only the reflections of the planes belonging to the cubic Cu_2O with the $Pn\bar{3}m$ space group can be observed when the temperature varies from 25°C to 280°C. However, through the Rietveld refinement, a certain percentage of the CuO phase is obtained (Table 3). The Rietveld refinement data show that the composition remains almost constant until the temperature reaches 280°C.

Above this temperature, the transformation begins, producing a mixture of the phases Cu_2O, CuO, and Cu. The samples heated from 280°C to 340°C show a peak at $2\theta = 42.88°$, indicating cubic copper with the $Fm\bar{3}m$ space group (COD card No. 96-901-3020). Moreover, the XRD shows two additional peaks at $2\theta = 35.54°$ and 38.69°, which belong to CuO planes (-111) and (111) of monoclinic CuO with the *C2*/c space group, respectively (PDF card No. 01-076-7800). Table 3 shows how the percentage of the phase of Cu_2O and

Cu decreases when the temperature ranges from 280°C to 340°C, while the phase CuO increases. At a temperature of 400°C, a mixture of the Cu_2O and CuO phases is observed with $45.49\% \pm 3.35\%$ and $54.51\% \pm 2.06\%$ proportions, respectively. Finally, at temperatures above 600°C, Cu_2O is oxidized and wholly transformed into CuO. Therefore, only the reflections belonging to CuO can be seen. The intensity of the peaks decreases when the temperature increases from room temperature to 700°C. This indicates that the crystallinity decreases when there is a conversion from Cu_2O to CuO, similar to the data reported by Amudhavalli et al. in 2018 [10].

From the *in-situ* temperature results, it can be guaranteed that the phase composition of the samples is maintained up to a temperature of 280°C. This could be beneficial for its potential use as a light-absorbing material for solar cells as well as its antibacterial properties [23, 24] since the particles maintain the Cu_2O phase in a more significant proportion and without any changes.

4. Conclusions

Cu_2O was obtained by a simple and rapid synthesis by reducing Benedict's solution with glucose without the need of any surfactants, sulfur-containing reagents, or catalysts. The sample with the largest amount of Cu_2O phase of $99.50\% \pm 0.34\%$ was synthesized with 7 g of glucose. The increment in the Cu_2O phase can be attributed to the increment in the glucose content in the reaction since it reduces more Cu^{+2} ions to Cu^{+1} ions forming Cu_2O. The glucose amount has a significant effect on reaction times. An atmosphere with an excess of glucose leads to a faster reaction, producing smaller crystallites with more microstrains. An atmosphere lacking glucose directs to a slower reaction, giving the crystallites a longer growth time which leads to a relaxation in the microstrains. The changes in morphology, such as cubes, irregular cubes, prismatic spheres, cauliflower-like, and spherical shapes, are also due to the reaction times, which are influenced by the glucose content in the synthesis. A fast reaction causes the particles to grow without any specific direction forming spheres, while a slow reaction leads to the growth in specific directions and the formation of cubes. The XPS spectra confirmed only the presence of chemical species such as Cu(I) and Cu(II). In addition, chemical defects such as oxygen vacancies (*Vo*) were detected in the samples. The Cu_2O shows a broad absorption range between 200 nm and 570 nm. The intensity absorption and band gap values remained almost constant regardless of the amount of glucose used. When analyzing the effect of the temperature in the *in-situ* X-ray diffraction, it became noticeable that the phase composition is maintained at temperatures up to 280°C, which could be advantageous for its potential use as a light absorber for second-generation solar cells.

Data Availability

The data used to support the findings of this study are available from the corresponding author upon request.

Conflicts of Interest

The authors declare that there is no conflict of interest regarding the publication of this paper.

Acknowledgments

The authors thank CIMAV Project [23011] for the support. We want to thank Jorge Domínguez, Ernesto Guerrero, César Leyva, and Luis de la Torre for their technical assistance.

References

[1] P. G. Vasconcelos Sampaio and M. G. Aguirre Orestes, "Photovoltaic solar energy: conceptual framework," *Renewable and Sustainable Energy Reviews*, vol. 74, pp. 590–601, 2017.

[2] S. Almosni, A. Delamarre, Z. Jehl et al., "Material challenges for solar cells in the twenty-first century: directions in emerging technologies," *Science and Technology of Advanced Materials*, vol. 19, no. 1, pp. 336–369, 2018.

[3] I. R. Hamdani and A. N. Bhaskarwar, "Cu_2O nanowires based p-n homojunction photocathode for improved current density and hydrogen generation through solar-water splitting," *International Journal of Hydrogen Energy*, vol. 46, no. 55, pp. 28064–28077, 2021.

[4] E. Rostami-Tapeh-Esmaeil, M. Golshan, M. Salami-Kalajahi, and H. Roghani-Mamaqani, "Synthesis of copper and copper oxide nanoparticles with different morphologies using aniline as reducing agent," *Solid State Communications*, vol. 334–335, pp. 1–9, 2021.

[5] J. Luceño-Sánchez, A. Díez-Pascual, and R. Peña Capilla, "Materials for photovoltaics: state of art and recent developments," *International Journal of Molecular Sciences*, vol. 20, no. 4, p. 976, 2019.

[6] A. Vasic, M. Vujisic, K. Stankovic, and P. Osmokrovic, "Characterization of thin films for solar cells and photodetectors and possibilities for improvement of solar cells characteristics," in *Solar Cells-Silicon Wafer-Based Technologies*, L. A. Kosyachenko, Ed., pp. 275–298, INTECH Open Access Publisher, 2012.

[7] M. D. Susman, Y. Feldman, A. Vaskevich, and I. Rubinstein, "Chemical deposition of Cu_2O nanocrystals with precise morphology control," *ACS Nano*, vol. 8, no. 1, pp. 162–174, 2014.

[8] S. Ghosh, S. R. Keshri, S. Bera, and R. N. Basu, "Enhanced solar hydrogen generation using Cu-Cu_2O integrated polypyrrole nanofibers as heterostructured catalysts," *International Journal of Hydrogen Energy*, vol. 45, no. 11, pp. 6159–6173, 2020.

[9] C. Ravichandiran, A. Sakthivelu, R. Davidprabu et al., "In-depth study on structural, optical, photoluminescence and electrical properties of electrodeposited Cu_2O thin films for optoelectronics: an effect of solution pH," *Microelectronic Engineering*, vol. 210, pp. 27–34, 2019.

[10] K. Amudhavalli, N. Neelakandapillai, and M. Nagarajan, "Synthesis of Cu_2O by SILAR and the impact of annealing on the structural properties," *International Journal of Management Science and Engineering Management*, vol. 3, pp. 494–497, 2018.

[11] A. Pérez-Tomás, A. Mingorance, D. Tanenbaum, and M. Lira-Cantú, "Metal oxides in photovoltaics: perovskite solar cells," in *The future of semiconductor oxides in next-generation solar cells*, M. Lira-Cantu, Ed., pp. 267–356, Elsevier Inc., 2018.

[12] S. S. Sawant, A. D. Bhagwat, and C. M. Mahajan, "Synthesis of cuprous oxide (Cu_2O) nanoparticles-a review," *Journal of Nano- and Electronic Physics*, vol. 8, no. 1, pp. 01035-1–01035-5, 2016.

[13] M. A. Badillo-Ávila, R. Castanedo-Pérez, M. A. Villarreal-Andrade, and G. Torres-Delgado, "Cu_2O thin films obtained at low temperature by mono- ethanolamine decomposition in open atmosphere," *Materials Science in Semiconductor Processing*, vol. 85, pp. 168–176, 2018.

[14] J. Zhu, N. Lu, W. Chen et al., "Influence of Au nanoparticle shape on Au@Cu_2O heterostructures," *Journal of Nanomaterials*, vol. 2015, Article ID 389790, 9 pages, 2015.

[15] D. Guo, L. Wang, Y. Du, Z. Ma, and L. Shen, "Preparation of octahedral Cu_2O nanoparticles by a green route," *Materials Letters*, vol. 160, pp. 541–543, 2015.

[16] M. Sabbaghan, J. Beheshtian, and R. N. Liarjdame, "Preparation of Cu_2O nanostructures by changing reducing agent and their optical properties," *Materials Letters*, vol. 153, pp. 1–4, 2015.

[17] E. Carbó-Argibay, X. Bao, C. Rodríguez-Abreu et al., "Up-scaling the synthesis of Cu_2O submicron particles with controlled morphologies for solar H_2 evolution from water," *Journal of Colloid and Interface Science*, vol. 456, pp. 219–227, 2015.

[18] D. Li, K. Dai, J. Lv, L. Lu, C. Liang, and G. Zhu, "Facile and large scale synthesis of novel Cu_2O octahedral crystals with efficient visible light photocatalytic activity," *Materials Letters*, vol. 150, pp. 48–51, 2015.

[19] V. Andal and G. Buvaneswari, "Preparation of Cu_2O nanocolloid and its application as selective colorimetric sensor for Ag^+ ion," *Sensors and Actuators B: Chemical*, vol. 155, no. 2, Article ID 825021, pp. 653–658, 2011.

[20] D. Lai, T. Liu, X. Gu et al., "Suspension synthesis of surfactant-free cuprous oxide quantum dots," *Journal of Nanomaterials*, vol. 2015, 8 pages, 2015.

[21] S. McWilliams, C. D. Flynn, J. McWilliams et al., "Nanostructured Cu_2O synthesized via bipolar electrochemistry," *Nanomaterials*, vol. 9, no. 12, pp. 1–16, 2019.

[22] Y. Wang and K. Zhou, "Effect of OH- on morphology of Cu_2O particles prepared through reduction of cu(II) by glucose," *Journal of Central South University*, vol. 19, no. 8, pp. 2125–2129, 2012.

[23] W. V. da Costa, B. da Silva Pereira, M. C. Montanha et al., "Hybrid materials based on cotton fabric-Cu_2O nanoparticles with antibacterial properties against S. aureus," *Materials Chemistry and Physics*, vol. 201, pp. 339–343, 2017.

[24] V. T. Nguyen and K. S. Trinh, "Effects of synthetic procedures and postsynthesis incubation pH on size, shape, and antibacterial activity of copper (I) oxide nanoparticles," *Journal of Chemistry*, vol. 2020, Article ID 9541934, 10 pages, 2020.

[25] C. Liang, Z. Yu, Z. Fengrui et al., "Copper salts mediated morphological transformation of Cu_2O from cubes to hierarchical flower-like or microspheres and their supercapacitors performances," *Scientific Reports*, vol. 5, pp. 1–7, 2015.

[26] L. A. Dahonog, M. S. D. De la Vega, and M. D. L. Balela, "pH-dependent synthesis of copper oxide phases by polyol method," *Journal of Physics Conference Series*, vol. 1191, pp. 012043–012045, 2019.

[27] T. D. Musho, C. Wildfire, N. M. Houlihan, E. M. Sabolsky, and D. Shekhawat, "Study of Cu_2O particle morphology on microwave field enhancement," *Materials Chemistry and Physics*, vol. 216, pp. 278–284, 2018.

[28] L. Kang, M. Zhou, H. Zhou, F. Zhang, Z. Zhong, and W. Xing, "Controlled synthesis of Cu_2O microcrystals in membrane dispersion reactor and comparative activity in heterogeneous Fenton application," *Powder Technology*, vol. 343, pp. 847–854, 2019.

[29] N. Kumar, S. S. Parui, S. Limbu, D. K. Mahato, N. Tiwari, and R. N. Chauhan, "Structural and optical properties of sol-gel derived CuO and Cu_2O nanoparticles," *Materials Today: Proceedings*, vol. 41, pp. 237–241, 2021.

[30] M. Chen, H. Zhu, X. Li et al., "The influence of atmosphere on electrical property of copper oxide nanoparticles," *Journal of Nanomaterials*, vol. 2014, Article ID 461269, 6 pages, 2014.

[31] X. Wang, M. Chen, Y. He, and J. Zhu, "Shape-controlled preparation of Cu_2O crystals and their growth mechanism," *Journal of Alloys and Compounds*, vol. 628, pp. 50–56, 2015.

[32] Y. Bai, T. Yang, Q. Gu, G. Cheng, and R. Zheng, "Shape control mechanism of cuprous oxide nanoparticles in aqueous colloidal solutions," *Powder Technology*, vol. 227, pp. 35–42, 2012.

[33] X. Han, F. Liao, Y. Zhang, Z. Yuan, H. Chen, and C. Xu, "Rapid and template-free synthesis of Cu_2O truncated octahedra using glucose as green reducing agent," *Materials Letters*, vol. 210, pp. 31–34, 2018.

[34] B.-E. Yeo, Y.-S. Cho, and Y.-D. Huh, "Evolution of the morphology of Cu_2O microcrystals: cube to 50-facet polyhedron through beveled cube and rhombicuboctahedron," *CrystEngComm*, vol. 19, no. 12, pp. 1627–1632, 2017.

[35] S. Sun, X. Song, Y. Sun, D. Deng, and Z. Yang, "The crystal-facet-dependent effect of polyhedral Cu_2O microcrystals on photocatalytic activity," *Science and Technology*, vol. 2, no. 5, pp. 925–930, 2012.

[36] M. S. Aguilar and G. Rosas, "Facile synthesis of Cu_2O particles with different morphologies," *Journal of Solid State Chemistry*, vol. 270, pp. 192–199, 2019.

[37] L. R. Ceja-Romero, L. Ortega-Arroyo, J. M. Ortega Rueda De León et al., "Green chemistry synthesis of nano-cuprous oxide," *IET Nanobiotechnology*, vol. 10, no. 2, pp. 39–44, 2016.

[38] H. R. Ong, M. R. Khan, R. Ramli, and R. M. Yunus, "Synthesis of copper nanoparticles at room temperature using hydrazine in glycerol," *Applied Mechanics and Materials*, vol. 481, pp. 21–26, 2013.

[39] V. Andal and G. Buvaneswari, "Effect of reducing agents in the conversion of Cu_2O nanocolloid to cu nanocolloid," *Engineering Science and Technology, an International Journal*, vol. 20, no. 1, pp. 340–344, 2017.

[40] M. Mallik, S. Monia, M. Gupta, A. Ghosh, M. P. Toppo, and H. Roy, "Synthesis and characterization of Cu_2O nanoparticles," *Journal of Alloys and Compounds*, vol. 829, pp. 154623–154626, 2020.

[41] A. Khan, A. Rashid, R. Younas, and R. Chong, "A chemical reduction approach to the synthesis of copper nanoparticles," *International Nano Letters*, vol. 6, no. 1, pp. 21–26, 2016.

[42] N. Zayyoun, L. Bahmad, L. Laânab, and B. Jaber, "The effect of pH on the synthesis of stable Cu_2O/CuO nanoparticles by sol-gel method in a glycolic medium," *Applied Physics A: Materials Science & Processing*, vol. 122, no. 5, pp. 1–6, 2016.

[43] M. M. Ferrer, G. S. L. Fabris, B. V. de Faria, J. B. L. Martins, M. L. Moreira, and J. R. Sambrano, "Quantitative evaluation of the surface stability and morphological changes of Cu_2O particles," *Heliyon*, vol. 5, no. 10, pp. e02500–e02507, 2019.

[44] Y. Cao, J. Fan, L. Bai, F. Yuan, and Y. Chen, "Morphology evolution of Cu_2O from octahedra to hollow structures," *Crystal Growth & Design*, vol. 10, pp. 232–236, 2010.

[45] Y. Cao, Y. J. Wang, K. G. Zhou, and Z. Bi, "Morphology control of ultrafine cuprous oxide powder and its growth mechanism," *Transactions of the Nonferrous Metals Society of China*, vol. 20, pp. s216–s220, 2010.

[46] J. Rodríguez-Carvajal, "Recent developments of the program FULLPROF," *Commission on powder diffraction (IUCr). Newsletter*, vol. 26, pp. 12–19, 2001.

[47] J. Walton, P. Wincott, N. Fairely, and A. Carrick, *Peak fitting with casa XPS: a casa pocket book*, Neal Fairley Casa Software Ltd, 2010.

[48] T. Dimopoulos, "All-oxide solar cells," in *The future of semiconductor oxides in next-generation solar cells*, M. Lira-Cantu, Ed., pp. 439–480, Elsevier Inc., 2018.

[49] D. Nath, F. Singh, and R. Das, "X-ray diffraction analysis by Williamson-Hall, Halder-Wagner and size-strain plot methods of CdSe nanoparticles- a comparative study," *Materials Chemistry and Physics*, vol. 239, pp. 122021–122029, 2020.

[50] S. Sarkar and R. Das, "Determination of structural elements of synthesized silver nano-hexagon from X-ray diffraction analysis," *Indian Journal of Pure and Applied Physics*, vol. 56, pp. 765–772, 2018.

[51] A. Khorsand Zak, W. H. Abd, M. E. Majid, and R. Y. Abrishami, "X-ray analysis of ZnO nanoparticles by Williamson-Hall and size-strain plot methods," *Solid State Sciences*, vol. 13, no. 1, pp. 251–256, 2011.

[52] V. Mote, Y. Purushotham, and B. Dole, "Williamson-Hall analysis in estimation of lattice strain in nanometer-sized ZnO particles," *Journal of Theoretical and Applied Physics*, vol. 6, no. 1, pp. 1–8, 2012.

[53] C. Ramesh, M. Hariprasad, V. Ragunathan, and N. Jayakumar, "A novel route for synthesis and characterization of green Cu_2O/PVA nano composites," *European Journal of Applied Engineering and Scientific Research*, vol. 1, pp. 201–206, 2012.

[54] M. Kooti and L. Matouri, "Fabrication of nanosized cuprous oxide using Fehling's solution," *Scientia Iranica*, vol. 17, pp. 73–78, 2010.

[55] J. Walton, P. Wincott, A. Carrick, and N. Fairely, *CASAXPS Orange Manual*, Neal Fairley Casa Software Ltd, 2009.

[56] S. Y. Ahn, K. Park, D. Choi, J. Park, Y. J. Kim, and H. S. Kim, "A study on the transition of copper oxide by the incorporation of nitrogen," *Electronics*, vol. 8, no. 10, p. 1099, 2019.

[57] B. Li, Y. Li, Y. Zhao, and L. Sun, "Shape-controlled synthesis of Cu_2O nano/microcrystals and their antibacterial activity," *Journal of Physics and Chemistry of Solids*, vol. 74, no. 12, pp. 1842–1847, 2013.

[58] M. Devaraj, R. Saravanan, R. Deivasigamani, V. K. Gupta, F. Gracia, and S. Jayadevan, "Fabrication of novel shape Cu and Cu/Cu_2O nanoparticles modified electrode for the determination of dopamine and paracetamol," *Journal of Molecular Liquids*, vol. 221, pp. 930–941, 2016.

[59] M. C. Biesinger, "Advanced analysis of copper X-ray photoelectron spectra," *Surface and Interface Analysis*, vol. 49, no. 13, pp. 1325–1334, 2017.

[60] L. Meda and G. F. Cerofolini, "A decomposition procedure for the determination of copper oxidation states in Cu-zeolites by XPS," *Surface and Interface Analysis*, vol. 36, no. 8, pp. 756–759, 2004.

[61] M. Zahmakiran, S. Özkar, T. Kodaira, and T. Shiomi, "A novel, simple, organic free preparation and characterization of water dispersible photoluminescent Cu_2O nanocubes," *Materials Letters*, vol. 63, no. 3-4, pp. 400–402, 2009.

[62] F. R. Xiu and F. S. Zhang, "Size-controlled preparation of Cu_2O nanoparticles from waste printed circuit boards by supercritical water combined with electrokinetic process," *Journal of Hazardous Materials*, vol. 233-234, pp. 200–206, 2012.

[63] S. S. Abdullahi, S. Güner, Y. Koseoglu, I. Murtala, B. I. Adamu, and M. Abdulhamid, "Simple method for the determination of band gap of a nanopowdered sample using Kubelka Munk theory," *Journal of the Nigerian Association of Mathematical Physics*, vol. 35, pp. 241–246, 2016.

[64] M. Singh, M. Goyal, and K. Devlal, "Size and shape effects on the band gap of semiconductor compound nanomaterials," *Journal of Taibah University for Science*, vol. 12, no. 4, pp. 470–475, 2018.